BS 2019 2-4 SEPT ROME 16th IBPSA INTERNATIONAL CONFERENCE AND EXHIBITION

INTERNATIONAL BUILDING PERFORMANCE SIMULATION ASSOCIATION

Exploring the Sky Longwave Radiance Distribution in the French Basque Country

Raphaël Nahon[1], Jairo Paz Acuña y Miño[1], Benoit Beckers[1]
[1]Urban Physics Joint Laboratory, Université de Pau et des Pays de l'Adour, E2S UPPA, Bayonne, France

Abstract

The atmospheric radiation has a significant impact on the outside surface temperatures, and so on the building heating and cooling loads and on the outdoor thermal comfort. It is considered isotropic in most of the thermal simulation programs, though sky thermography shows that it is strongly anisotropic in the absence of clouds, with a gradient from the zenith to the horizon.

The main objective of this work is to propose a model for the sky temperature distribution under all-weather. Its originality is to propose thermograms of the complete sky vault under typical weather conditions.

The observed sky temperature distributions are compared to the results of the models by Bliss (1961) and Martin and Berdhal (1984a). The latter allowed for a correlation coefficient higher than 92% for five of the six analyzed sky conditions.

The comparison between the radiant power absorbed by a vertical surface at the Earth level using this model or considering an isothermal sky shows differences of up to 16%, resulting in differences of up to 3.5°C in the mean radiant temperature.

Introduction

The sky vault may be assimilated to a blackbody, characterized by its *temperature*, or to a grey body at the air temperature, characterized in this case by its *emissivity*. Atmospheric radiation, the longwave (wavelength superior to 4µm) radiant power emitted by the sky vault, has a significant impact on building heating and cooling loads and determines the potential of radiative cooling (Argiriou, 1992; Clark, 1981; Zeyghami, 2018). It contributes to the 3D radiant environment and influences outdoor thermal comfort.

Building simulation programs treat the atmospheric radiation as *isotropic*: the sky longwave radiance is supposed equal in every direction. In reality, it increases with the zenith angle, especially for clear and cold skies. Taking into account this variation is particularly relevant for the estimation of the performance of angularly or spectrally selective radiative cooling systems (Martin and Berdhal, 1984a); for the precise evaluation of the radiant environment in an urban context; or in the aim of reproducing thermograms through modelling (Aguerre, 2019).

In a previous paper (Nahon, 2016), the authors proposed to use the model described by Bliss (1961) and more recently used and discussed in (Awanou, 1998; Berger, 2003). Though this formulation of the sky emissivity variation with the zenith angle is constructed for a clear sky, it allows for a good representation of the sky pattern both for clear and dark overcast skies. It was therefore proposed to prefer this model than an isotropic one under all-weather, though the lack of data made difficult a discussion on the results. Another candidate would have been the model by Martin and Berdhal (1984a), which allows for a good correlation with fifty thousand of observations at five zenith angles between 1979 and 1980 at six U.S. locations, both under clear and cloudy skies.

The sky emissivity may be deduced from the sky *bright temperature* obtained by thermography (Kruczek, 2015). This technique allows for analyzing the sky temperature distribution with a great resolution, and the main originality of this work is to propose thermograms of the whole sky vault under six representative sky conditions. The shots were taken between November and December 2018, in Anglet, in the French Basque Country. The local weather is characterized by the quick alternation of clear and cloudy skies, which allowed us for capturing different representative sky types on a lapse of three days.

The main objective of this study is to discuss the use of the models by Bliss and Martin and Berdhal under all-weather. The observed and modelled sky temperatures are compared for six representative skies. The differences between the longwave irradiance on a vertical surface obtained from the pictures, and using an anisothermal and isothermal skies are analyzed. The resulting differences on the estimation of the mean radiant temperature under an extremely low sky emissivity are evaluated.

Using both models, the directional sky emissivity is estimated from the global sky emissivity, which can be measured or modelled. In most cases, measurements are not available in the weather data files used by building simulation programs, and the use of a model is necessary. A recent critical review on the subject can be found in Evangelisti (2019). Most of the models are constructed for clear skies, and only a few allows for considering cloud cover. In this study, the global sky emissivities deduced from the thermograms are compared to the formulation by Angström (1915) and Martin and Berdhal (1984b), here again with the objective of discussing their use regarding the data commonly used in building simulation programs.

https://doi.org/10.26868/25222708.2019.210351

Methods

Experimental set-up

Sky thermography was performed using an infrared (IR) camera (FLIR T460) set on a programmable robotic panoramic head (CLAUSS RODEON piXplorer) placed on a scaffolding on the top of a three-storey building located in Anglet, in the French Basque Country. The whole sky vault thermograms were obtained through the assembly of eight images: seven taken with a zenith angle of 60° plus one facing the zenith (cf. Figure 1).

Each of the thermograms is taken within ten to twenty seconds. A lens (FLIR T197412) with a field of view of 90 x 73° was used to limit the necessary number of thermograms, and therefore the delay between the first and last shots. The apparent temperature near the edges of the thermograms is incorrect, and, though five thermograms would have been enough, it would have induced errors due to distortion and vignetting effect. The use of eight thermograms appears as a good compromise between the delay and the precision.

The sky vault is modelled as a hemisphere discretized in *tiles*. The temperature of each tile is taken from the pixel the closest to its center. We use the partition scheme described by Beckers (2014), which allows us to freely choose the number of tiles and ensures that each of them has the same solid angle and aspect ratio. Doing so, the maximum angular displacement between the center of a tile and its boundary is nearly constant and controlled. A partition in 100 000 tiles was used to generate the images while 5000 tiles are more than sufficient for the calculations. The resolution of the IR camera is 320 x 240 pixels. Only 16% of the total 614 400 pixels were used and a lower resolution would have been sufficient.

In total, 40 sky thermograms were taken on 9 different days from November 15 to December 11, 2018. Only six of the resulting pictures are presented in this paper. Each of them goes along with a whole sky vault photograph, constructed in the same way, using in this case a camera with a field of view of 75.3 x 59.3°. Air temperature and relative humidity at the time of the shooting were measured on site.

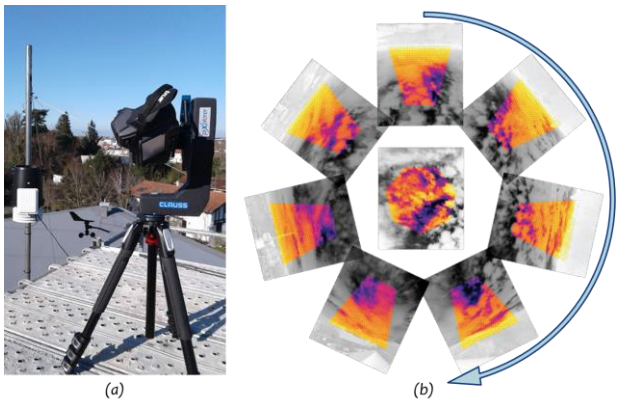

Figure 1: (a) experimental setup and (b) resulting thermograms

Measurement of the sky thermal radiation using an IR camera

Setting the distance to the measured object and its emissivity to one, the IR camera converts the total radiation beam seen by the IR detector into the temperature of blackbody. The IR detector of the camera is sensitive on the spectral range 7.5 to 13 µm, which includes the *atmospheric window*. Between 8 to 13 µm, the atmosphere does not behave as a blackbody and its emissivity depends mostly on its water vapour content: it is merely transparent for dry conditions and behaves as a blackbody for an important relative humidity. Because of this phenomenon, the bright temperature given by the IR camera has to be corrected to obtain the real sky temperature. To do so, the longwave radiant power reaching the camera is calculated by integrating Planck's formula between 4 to 100 µm, using: 1) the bright temperature inside the atmospheric windows (between 4.5 to 4.8 µm and between 7.5 to 13 µm) and 2) the air temperature on the remaining spectrum (Kruczek, 2015).

Less than 5% of the sky vault is obstructed by faraway trees and by the vertical arm of the nearby weather station. This fraction of the sky view factor from a horizontal surface is limited to 0.5%, and so is its contribution to the horizontal longwave irradiance. While exposed to the sun, these objects can reach a temperature superior to that of the air. The sky cannot, and it is set to the air temperature wherever it is exceeded.

The result of these corrections is illustrated in Figure 2: while the sky temperature ranges from -36 to 14°C in the original thermogram, its variation is limited to -6 to 12°C after corrections.

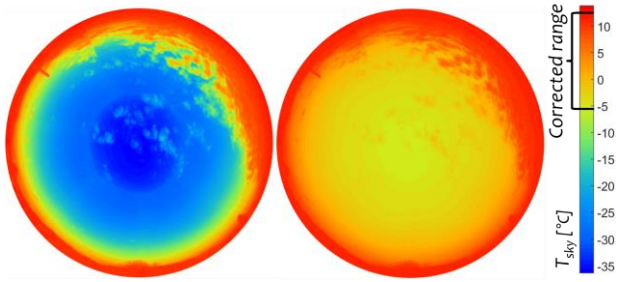

Figure 2: Equivalent projection of the original and corrected sky vault thermograms (December 4 at 8:50, Ta=12°C)

The IR camera offers different temperature ranges. Sky thermograms were obtained using the lowest one, from -20 to 120°C. In this configuration, the maximal temperature given by the camera is 150°C. The sun bright temperature exceeds this value. Selecting the highest range of temperature, from 250 to 1500°C, the sun bright temperature is 1013°C (cf. Figure 3). Meanwhile, due to its low view factor, its contribution to IR horizontal irradiance is negligible.

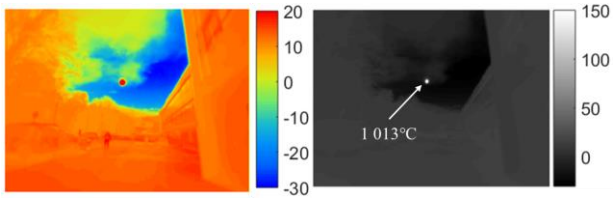

Figure 3: Sun bright temperature on a thermogram for different temperature ranges

Modelling the sky thermal radiation

The models by Bliss (1) and Martin and Berdhal (2) for the variation of the sky emissivity with the zenith angle are used. Both of them express the directional sky emissivity ε_θ as a function of the global sky emissivity ε_s and a dimensionless coefficient b_i :

$$\varepsilon_\theta = 1 - (1 - \varepsilon_s)^{1 / (\, b_1 \cos\theta\,)} \quad (1)$$

$$\varepsilon_\theta = 1 - (1 - \varepsilon_s)\, e^{\, b_2 (1.7 - 1 / \cos\theta\,)} \quad (2)$$

While the first one was constructed for a clear sky, the second showed a good correlation under all sky conditions. The integration of ε_θ on the hemisphere must equal ε_s and, in both cases, the coefficient b_i is implicitly dependent on the global sky emissivity. Bliss (1961) uses a constant value of 1.8 to minimize the error for low emissivity skies. Martin and Berdhal (1984a) use a varying parameter. Hereafter, the coefficients b_i are established by iterations: the value of b_i which minimizes the difference $\Delta\varepsilon$ between the integration of ε_θ on the hemisphere and ε_s is taken in each case. Values ranging from 1.3 to 1.7 with a step of 0.01 are tested for b_1; ranging from 0.30 to 0.4 with a step of 0.005 for b_2. Doing so, $\Delta\varepsilon$ is limited to 0.05%.

Comparison of the sky thermograms and modelled sky temperatures

The above described models use as only input the sky global emissivity. The latter can be measured using pyrgeometer or modelled. It is deduced from the thermograms for the comparison of the modelled and observed sky directional emissivity.

Results

Sky thermograms vs modelled sky temperatures

Six of the forty conducted sky thermograms are selected and compared to the modelled sky temperatures (Figure 4figures 4 to 6). The curves have been created by comparing the modelled and observed sky emissivity for the north facing tiles marked by a white line on the figures. The model from Bliss gives unsatisfying results in almost every case and the comparison is focused on the model by Martin and Berdhal.

The first two shots (Figure 4) were taken on December 7, the first one at 13h20 and the second at 14h35. In the first case, the sky is completely free of clouds, the air is at 16.7°C and the relative humidity is 50%. In the second, barely more than an hour later, the sky is completely overcast by low cumulus. The air temperature and relative humidity have not changed much, with respectively 15.9°C and 54%. In both cases, the model gives consistent results, with a maximal and mean difference between the modelled and observed sky emissivity respectively of 6.3 and 2.4 points in the first and of 2.7 and 0.9 points in the second. Note that, in every case, the modelled sky emissivity is slightly inferior to the observed one for zenith angles lower than 54° and then the slightly superior, the biggest differences occurring near the horizon.

The two following shots (Figure 5), were taken on December 4 and 5, at respectively 12h10 and 10h10. In the first one, the sky is overcast by high and bright cirrus clouds, the air is at 16.4°C and the relative humidity is 89%. The second one was taken under a dense fog. Here again, the model gives compelling results, with a maximal and mean difference respectively of 5 and 1.4 in the first case and of 1.3 and 0.3 points in the second. In both cases the maximal difference occurs at the horizon.

The two final shots (Figure 6) were taken under intermediate skies, on December 4 at 8h50 and 10h30. In the first one, low opaque clouds are visible near the horizon and high thin clouds are scattered close to the zenith. In the second, low opaque clouds are scattered over the entire sky vault. In the first case, the modelled sky emissivity matches the observed one, especially for zenith angle lower than 54°, with maximal and mean differences of respectively 7.2 and 1.4 points. In the second one, both models fail to predict the erratic variations of the sky emissivity, with the alternation of opaque cumulus and blue sky. Meanwhile, the difference between the modelled and observed sky emissivity is limited to 5.7 points, with a mean of 2.7 points. Cloud positions being impossible to predict, it seems difficult to reach a better correlation under partially overcast skies. Besides, the error is comparable considering an isotropic sky, and it seems reasonable to prefer the model by Martin and Berdhal (1984a) even in those particular cases.

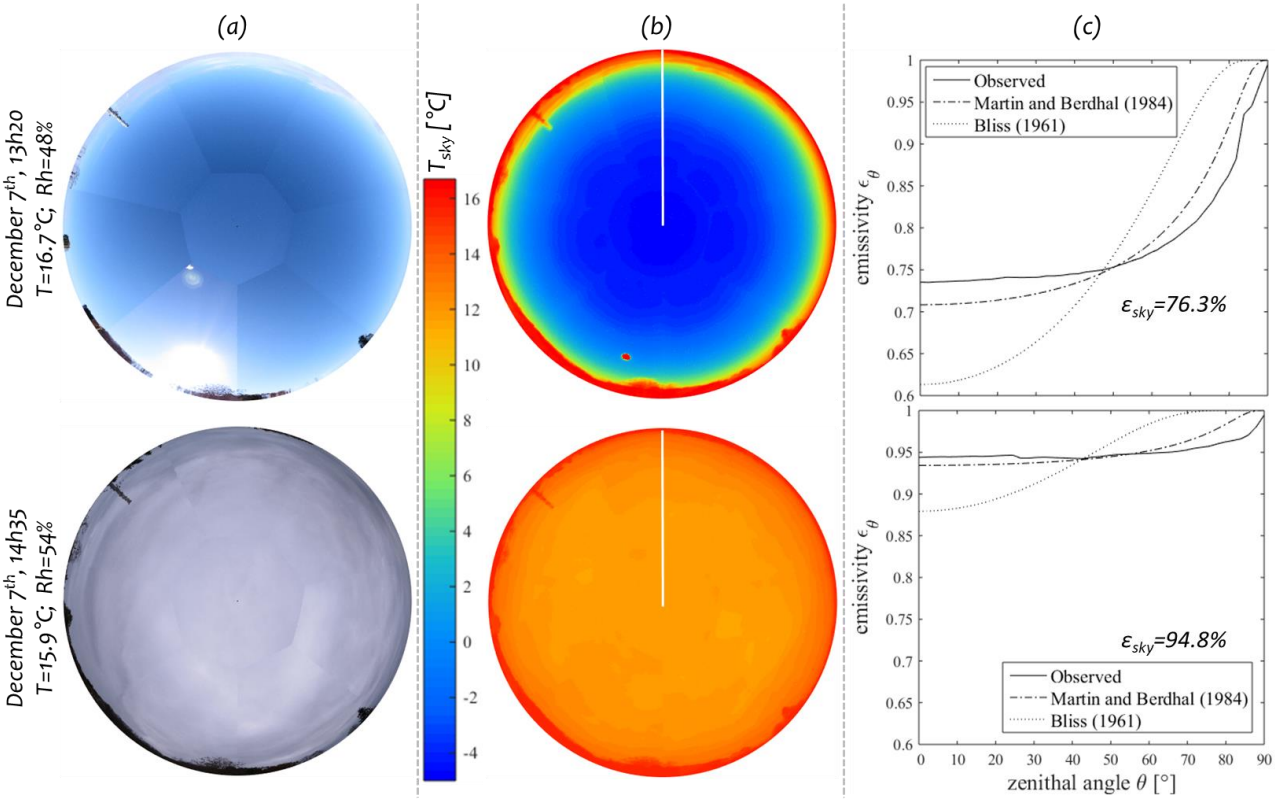

Figure 4: Clear and dark overcast skies: Equivalent projection of the sky (a) photographs and (b) corrected thermograms; (c) comparison between the observed and modelled sky emissivity

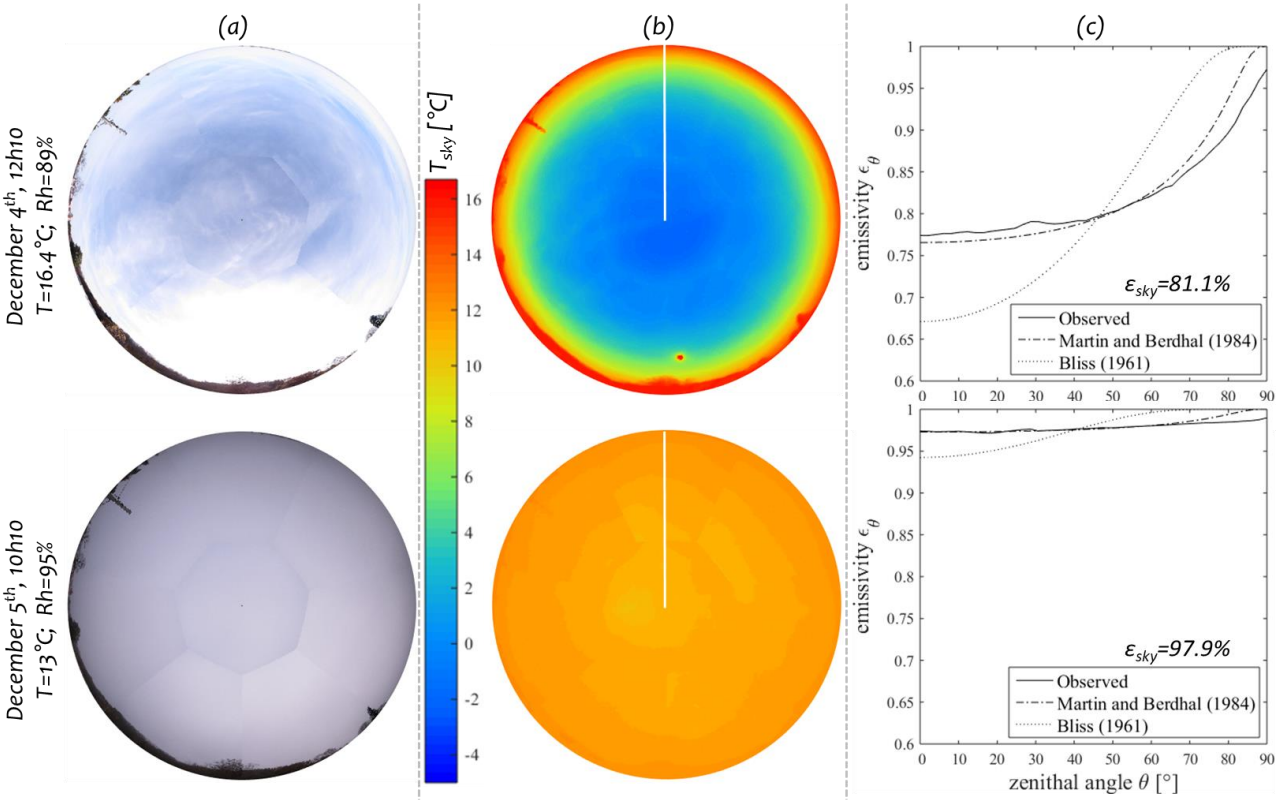

Figure 5: Bright overcast and foggy skies: Equivalent projection of the sky (a) photographs and (b) corrected thermograms; (c) comparison between the observed and modelled sky emissivity

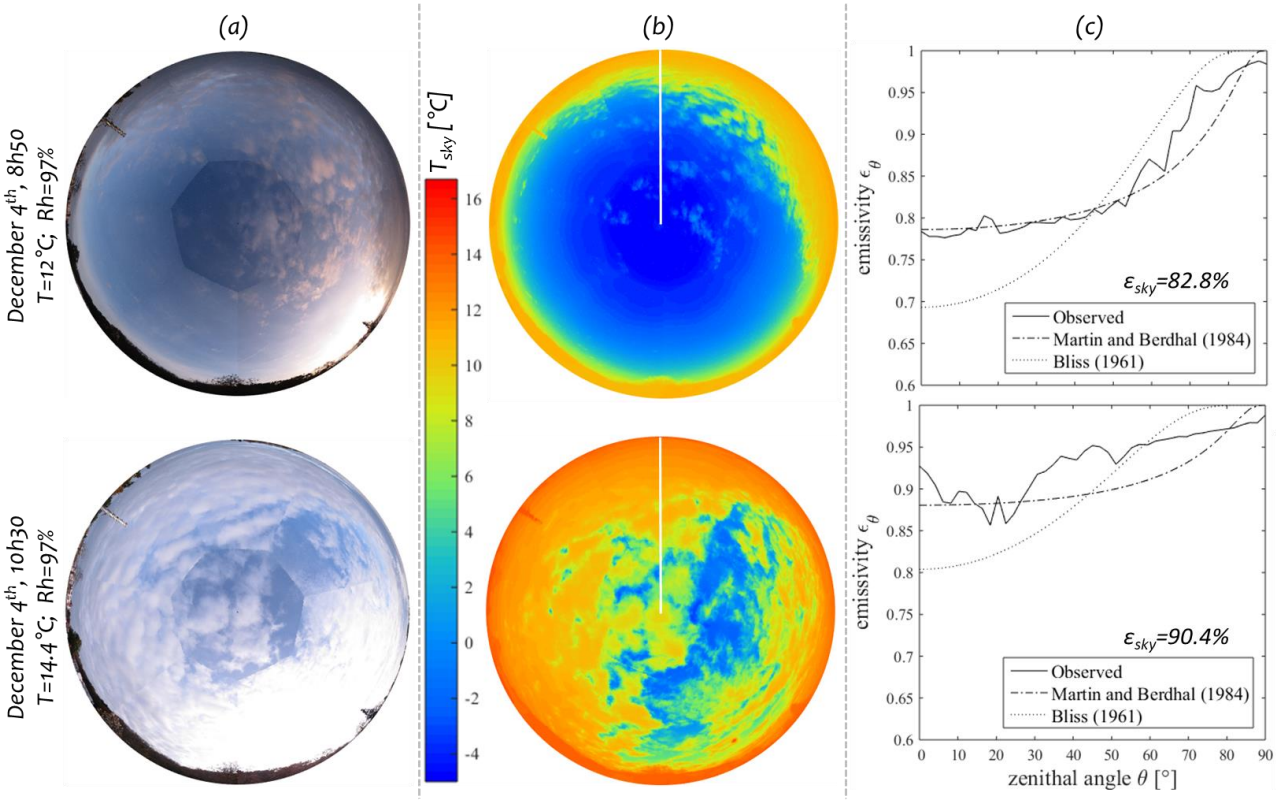

Figure 6: Partly and mostly cloudy skies: Equivalent projection of the sky (a) photographs and (b) corrected thermograms; (c) comparison between the observed and modelled sky emissivity

Impact of the sky anisotropy on the LW vertical irradiance

The longwave irradiance on a north facing wall is first computed using the observed sky temperature for the six sky types discussed in the above section. This reference value is then compared to that obtained using the model from Martin and Berdhal (1984a) and considering an isotropic sky (cf. Figure 7).

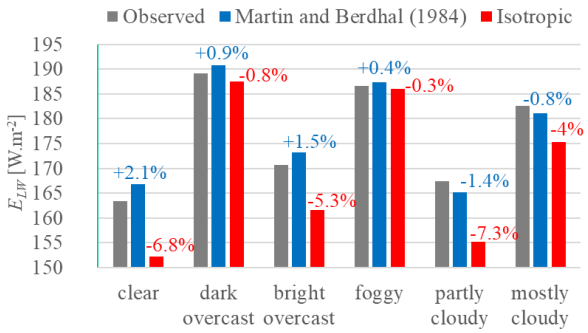

Figure 7: Longwave irradiance (E_{LW}) on a North facing vertical surface. (Relative differences between observed and modelled irradiances are stated directly on the picture)

The relative difference between the observed and modelled longwave irradiance is limited to 2.1% using the model from Martin and Berdhal (1984a) while it reaches -7.3% considering an isotropic sky. Both models give pretty good results in the case of a dark overcast and foggy skies, with relative differences of -0.8 and +0.9% in the first case and -0.3 and +0.4% in the second. For the other sky types, using the model from Martin and Berdhal (1984a) allows for the reduction of the difference between the modelled and observed longwave irradiances by 3 to 6%.

Impact of the sky anisotropy on the mean radiant temperature under a dry climate

The impact of the sky anisotropy on the radiative environment is higher for low emissivity skies, characteristic of cold and dry climates. The city of Montreal, Canada, is known for its very dry winter. The mean radiant temperature is calculated as described by Lindberg (2008) for the night with the lowest sky emissivity, on February 27th at 19h30, using the *Typical Meteorological Year* (TMY) from the international airport of Montreal freely available on the EnergyPlus website (energyplus.net/weather). The air temperature is -16.1°C, the relative humidity is 40%. The sky global emissivity is calculated using the model described by Martin and Berdhal (1984a) for a dew point temperature -25.6°C. The ground is supposed at the air temperature and its emissivity is set to one. Considering a uniform sky emissivity, the mean radiant temperature is -24.2°C, while it is more than 3.5°C superior taking into account its variation with the zenith angle. The sky vertical irradiance is 16% (91 vs 77 $W.m^{-2}$) higher taking into account the sky anisotropy, which explains the difference.

Discussion

As mentioned before, the coefficient b_2 from the model by Martin and Berdhal (1984a) is calculated by iterations to minimize the difference $\Delta\varepsilon$ between the integration of ε_θ on the hemisphere and the global sky emissivity ε_s. The

values obtained with a step of 0.001 for a wide range of sky emissivities are displayed in Figure 8. The variation of the coefficient is limited for ε_s inferior to 90%. Besides, the higher is ε_s, the lower is the impact of the b_2 coefficient on the sky directional emissivity (cf. equation (2)). For these reasons, using a constant coefficient of 0.308 allows for the limitation of $\Delta\varepsilon$ to 0.015%, which appears more than reasonable.

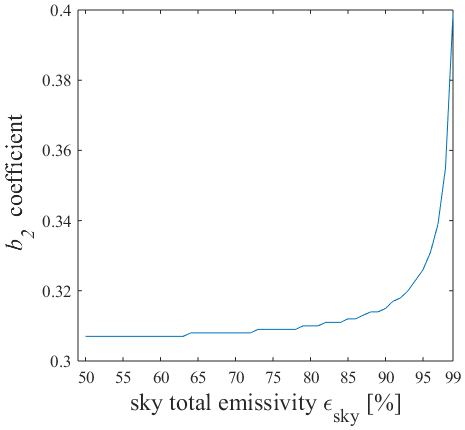

Figure 8: Values of the b_2 coefficient for a wide range of sky emissivities

The correct evaluation of the sky global emissivity is determinant to achieve a good description of the sky longwave radiance distribution. Building simulation programs generally use weather data representative of the local climate such as TMY. Each of the data is associated to an 'uncertainty flag code' (Crawley, 1999). On the one hand, the horizontal infrared irradiance is usually associated with the flag '?0', which corresponds to a datum of unknown source with an uncertainty higher than 50%. On the other hand, the air and dew point temperature as well as the ceiling height, opaque and total sky cover are usually associated with the flag 'A7', which corresponds to measured data with an 'uncertainty consistent with NWS practices and the instrument or observation used to obtain the data'. We therefore recommend not to use the diffuse horizontal irradiance but to estimate ε_s from the measured air temperature and cloud cover. As mentioned in the introduction, a review of the existing models can be found in (Evangelisti, 2019). Here, we choose to use the widely used model described by Martin and Berdhal (1984b) and the one described in the pioneer work by Angström (1915). Both models allow for clouds consideration. The first distinguishes opaque and thin clouds:

$$\varepsilon_s = \varepsilon_o + (1 - \varepsilon_o) (N_1 \varepsilon_{c1} e^{h1 / ho} + N_2 \varepsilon_{c2} e^{h2 / 8.2}) \quad (3)$$

with N_1 and N_2 the fractional area covered by respectively opaque and thin clouds, estimated in our case from the thermograms; $\varepsilon_{c1} = 1$ and $\varepsilon_{c2} = 0.4$ default opaque and thin cloud emissivities; $h_1 = 2$ km and $h_2 = 8$ km opaque and thin cloud base heights; ε_o the clear sky emissivity, as defined in the model by Berdhal and Martin (1984):

$$\varepsilon_o = 0.711 + 0.56\,(Td/100) + 0.73(Td/100)^2 + \Delta\varepsilon_h \quad (4)$$

with Td the dew point temperature [°C] and $\Delta\varepsilon_h = 0.013 \cos(2\pi\, t/24)$ the diurnal correction, t being the solar time in hour.

The second takes into account only the opaque sky cover:

$$\varepsilon_s = (0.82 - 0.25\text{x}10^{-0.0945\, Vp}) (1 + 0.21\, N_1^{\,2.5}) \quad (5)$$

with V_p [hPa] the water vapor pressure, which is deduced from the measured air temperature Ta [°C] and relative humidity rH [%] using the Arden Buck (1981) formulation:

$$V_p = \text{rH}/100\text{x}6.1121\, e^{18.678\, -\, Ta\, /\, 234.4)\ \ Ta\, /\, (257.14+Ta)} \quad (6)$$

The values obtained using those two models are compared in Figure 9 to the sky emissivities deduced from the thermograms.

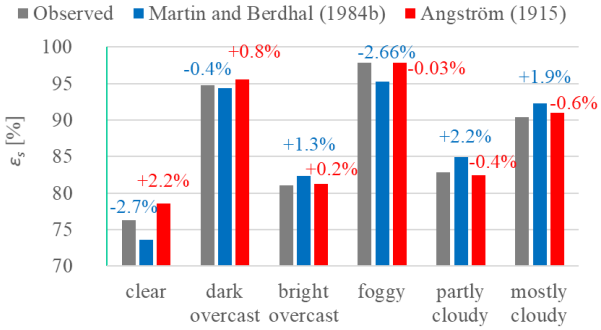

Figure 9: Global sky emissivity [%] (Absolute differences are stated directly on the figure)

Both models give satisfying results for every of the sky types analyzed in this paper, with a maximal difference between the observed and modelled sky emissivity of 2.7 points. Note that the results from the model by Angström are closer to the observed sky emissivities in almost every case, with an absolute difference inferior to 1% for five of the six analyzed skies.

Conclusion

In this paper, modelled sky temperatures are compared to whole sky vault thermograms. The observation campaign took place in the French Basque Country from November to December 2018. Six different sky types are analyzed. Two models (Bliss, 1961; Martin and Berdhal, 1984a) for the variation of the sky emissivity with the zenith angle are used for the comparison.

While the first one gives unsatisfying results for the chosen days and locality, the sky emissivity obtained using the model from Martin and Berdhal fits well with the observed one. The correlation coefficient is superior to 92% in every case except for the 'mostly cloudy' (78%) sky.

The modelled and observed longwave irradiances on a vertical surface are compared. It is shown that the error resulting from the consideration of an isotropic sky is reduced by up to 6% using the model from Martin and Berdhal.

The impact of sky anisotropy on the vertical longwave irradiance and resulting mean radiant temperature for a very low sky emissivity is illustrated. It is shown that, for a mean sky emissivity of 62%, the longwave vertical irradiance is 16% higher using the proposed model than considering an isotropic sky, which leads to an error of 3.5°C on the mean radiant temperature.

Finally, the model's *b* coefficient value (cf. equation (2)) is discussed. It is proposed to use a constant value of 0.308, which limits the resulting error on the global sky emissivity to 0.015%. The observed global sky emissivities for the six typical skies are compared to the models by Angström (1915) and Martin and Berdhal (1984b). Both of them produce satisfying results, with a maximum difference of 2.7% for the six representative skies analyzed in this paper. The first one is systematically closer in this case, with a difference inferior to 1% for five of the six skies.

In short, it is proposed to use model by Martin and Berdhal (1984a) with b=0.308 under all weather conditions, using as input the global sky emissivity given by (Angström, 1915). The implantation of the proposed model is easy and the associated calculation costs are null. It allows for a better representation of the actual sky longwave radiance distribution than an isotropic one and consequently reduces related errors. The experimental campaign was limited to three days in only one location and further investigations are required to confirm that these conclusions can be generalized to all-weather conditions and localities. Nevertheless, it seems reasonable to prefer the proposed model to an isotropic one, everywhere and for all kind of applications.

References

Aguerre, J., Nahon, R., Garcia-Nevado, E., La Borderie, C., Fernández, E., and Beckers, B. (2019). A street in perspective: Thermography simulated by the finite element method. *Building and Environment 148*, 225–239.

Angstöm, A. (1915). A study of the radiation of the atmosphere. Based upon observations of the nocturnal radiation during expeditions to Algeria and to California. *Smithsonian Miscellaneous Collections 65*(3).

Argiriou, A., Santamouris, M., Balaras, C. and Jeter, S. (1992). Potential of radiative cooling in southern Europe. *International Journal of Solar Energy 13*, 189-203.

Awanou, C.N. (1998). Clear sky emissivity as a function of the zenith direction. *Renewable Energy 13*(2), 227–248.

Beckers, B. and Beckers, P. (2014). Sky vault partition for computing daylight availability and shortwave energy budget on an urban scale. *Lighting Research and Technology 46*(6), 716–728.

Berdahl, P. and Martin, M. (1984). Emissivity of clear skies. *Solar Energy 32*, 663–664.

Berger, X. and Bathiebo, J. (2003). Directional spectral emissivities of clear skies. *Renewable Energy 28*, 1925–1933.

Bliss, R.W. (1961). Atmospheric radiation near the surface of the ground. *Solar Energy 5*(3), 103–20.

Clark, G. (1981). Passive/hybrid comfort cooling by thermal radiation. *Proceedings from the International passive and hybrid cooling conference*. Miami Beach (U.S.A.), 9 November 1981.

Crawley, D.B., Hand, J.W. and Lawrie, L.K. (1999). Improving the Weather Information Available to Simulation Programs. *Proceedings from the Sixth International IBPSA Conference (BS '99)*. Kyoto (Japan), 13-15 September 1999.

Kruczek, T. (2015). Use of infrared camera in energy diagnostics of the objects placed in open air space in particular at non-isothermal sky. *Energy 91*, 35–47.

Lindberg, F., Holmer, B., and Thorsson, S. (2008) SOLWEIG 1.0 – Modelling spatial variations of 3D radiant fluxes and mean radiant temperature in complex urban settings. *International Journal of Biometeorology 52*, 697–713.

Nahon, R., Blanpain, O. and Beckers, B. (2016). Impact of the anisotropy of the sky vault emissivity on the building envelope radiative budget. *Proceedings from FICUP2016: First International Conference on Urban Physics*, Quito – Galápagos (Ecuador), 26-30 September 2016.

Martin, M. and Berdhal, P. (1984a). Summary of results from the spectral and angular sky radiation measurement program. *Solar Energy 33*(3/4), 241–252.

Martin, M. and Berdhal, P. (1984b). Characteristics of infrared sky radiation in the united states. *Solar Energy 33*(3/4), 321–336

Zeyghami, M., Yogi Goswami, D., Stefanakos, E. (2018) A review of clear sky radiative cooling developments and applications in renewable power systems and passive building cooling. *Solar Energy Materials and Solar Cells 178*, 115–128